The Astrophysical Journal, 944:58 (7pp), 2023 February 10 https://doi.org/10.3847/1538-4357/acaec6

The Hubble Space Telescope UV Legacy Survey of Galactic Globular Clusters. XXIV. Differences in Internal Kinematics of Multiple Stellar Populations

Mattia Libralato[1], Enrico Vesperini[2], Andrea Bellini[3], Antonino P. Milone[4,5], Roeland P. van der Marel[3,6], Giampaolo Piotto[4,5], Jay Anderson[3], Antonio Aparicio[7,8,9], Beatriz Barbuy[10], Luigi R. Bedin[5], Thomas M. Brown[3], Santi Cassisi[11,12], Domenico Nardiello[5], Ata Sarajedini[13], and Michele Scalco[2,5,14]

[1] AURA for the European Space Agency (ESA), Space Telescope Science Institute, 3700 San Martin Drive, Baltimore, MD 21218, USA; libra@stsci.edu
[2] Department of Astronomy, Indiana University, Bloomington, IN 47405, USA
[3] Space Telescope Science Institute 3700 San Martin Drive, Baltimore, MD 21218, USA
[4] Dipartimento di Fisica e Astronomia, Università di Padova, Vicolo dell'Osservatorio 3, Padova, I-35122, Italy
[5] INAF—Osservatorio Astronomico di Padova, Vicolo dell'Osservatorio 5, Padova, I-35122, Italy
[6] Center for Astrophysical Sciences, The William H. Miller III Department of Physics & Astronomy, Johns Hopkins University, Baltimore, MD 21218, USA
[7] Instituto de Astrofísica de Canarias, Calle Vía Láctea, La Laguna, Tenerife, Canary Islands, E-38205, Spain
[8] Departamento de Astrofísica, Universidad de La Laguna, Av. Astrofśico Francisco Sánchez, La Laguna, Tenerife, Canary Islands, E-38206, Spain
[9] Department of Aerospace Engineering, Khalifa University of Science and Technology, P.O. Box 127788, Abu Dhabi, United Arab Emirates
[10] Universidade de São Paulo, IAG, Rua do Matão 1226, Cidade Universitásria, São Paulo 05508-900, Brazil
[11] INAF—Osservatorio Astronomico di Abruzzo, Via M. Maggini, s/n, Teramo, I-64100, Italy
[12] INFN—Sezione di Pisa, Largo Pontecorvo 3, Pisa, I-56127, Italy
[13] Department of Physics, Florida Atlantic University, Boca Raton, FL 33431, USA
[14] Dipartimento di Fisica e Scienze della Terra, Università di Ferrara, Via Giuseppe Saragat 1, Ferrara, I-44122, Italy
Received 2022 November 16; revised 2022 December 17; accepted 2022 December 20; published 2023 February 13

Abstract

Our understanding of the kinematic properties of multiple stellar populations (mPOPs) in Galactic globular clusters (GCs) is still limited compared to what we know about their chemical and photometric characteristics. Such limitation arises from the lack of a comprehensive observational investigation of this topic. Here we present the first homogeneous kinematic analysis of mPOPs in 56 GCs based on high-precision proper motions computed with Hubble Space Telescope data. We focused on red-giant-branch stars, for which the mPOP tagging is clearer, and measured the velocity dispersion of stars belonging to first (1G) and second generations (2G). We find that 1G stars are generally kinematically isotropic even at the half-light radius, whereas 2G stars are isotropic at the center and become radially anisotropic before the half-light radius. The radial anisotropy is induced by a lower tangential velocity dispersion of 2G stars with respect to the 1G population, while the radial component of the motion is comparable. We also show possible evidence that the kinematic properties of mPOPs are affected by the Galactic tidal field, corroborating previous observational and theoretical results suggesting a relation between the strength of the external tidal field and some properties of mPOPs. Although limited to the GCs' central regions, our analysis leads to new insights into the mPOP phenomenon, and provides the motivation for future observational studies of the internal kinematics of mPOPs.

Unified Astronomy Thesaurus concepts: Globular star clusters (656); Proper motions (1295); Stellar kinematics (1608)

1. Introduction

The puzzle of the origin of the multiple stellar populations (mPOPs) in Galactic globular clusters (GCs) has been controversial since their discovery. The large amount of spectroscopic and photometric data collected so far has provided almost all observational information we know about mPOPs in GCs, but no definitive consensus has been reached yet about the formation and evolution of mPOPs (Gratton et al. 2012, 2019; Renzini et al. 2015; Bastian & Lardo 2018; Cassisi & Salaris 2020; Milone & Marino 2022). The interplay between theoretical and observational efforts has pushed the community to find new ways to constrain the origin of mPOPs in GCs. For example, this research field is progressively seeking answers by looking at young and massive clusters in other galaxies (e.g., Larsen et al. 2014; Dalessandro et al. 2016; Niederhofer et al. 2017; Lagioia et al. 2019; Nardiello et al. 2019; Martocchia et al. 2019; Milone et al. 2020). However, there is still an almost uncharted wealth of information in Galactic GCs that can enrich the observational picture of mPOPs: their internal kinematics.

Here, we investigate the kinematic properties of first (1G) and second (2G) generation stars hosted in GCs. This effort focuses on red-giant branch (RGB) stars, for which the separation between different populations is clearer. We make use of the homogeneous collection of proper montions (PMs) obtained with Hubble Space Telescope (HST) data recently published by Libralato et al. (2022, hereafter L22) for 56 globular and one open clusters, and compare the properties of the velocity distributions of 1G and 2G stars.

The outline of the paper is the following. Section 2 describes the data sets used for this study, the procedure to identify the mPOPs, and how we calculated their kinematic properties. Section 3 reports our results concerning the kinematics of mPOPs; while in Section 4 we investigate the possible dependence of the velocity anisotropy on the Galactic tidal field.

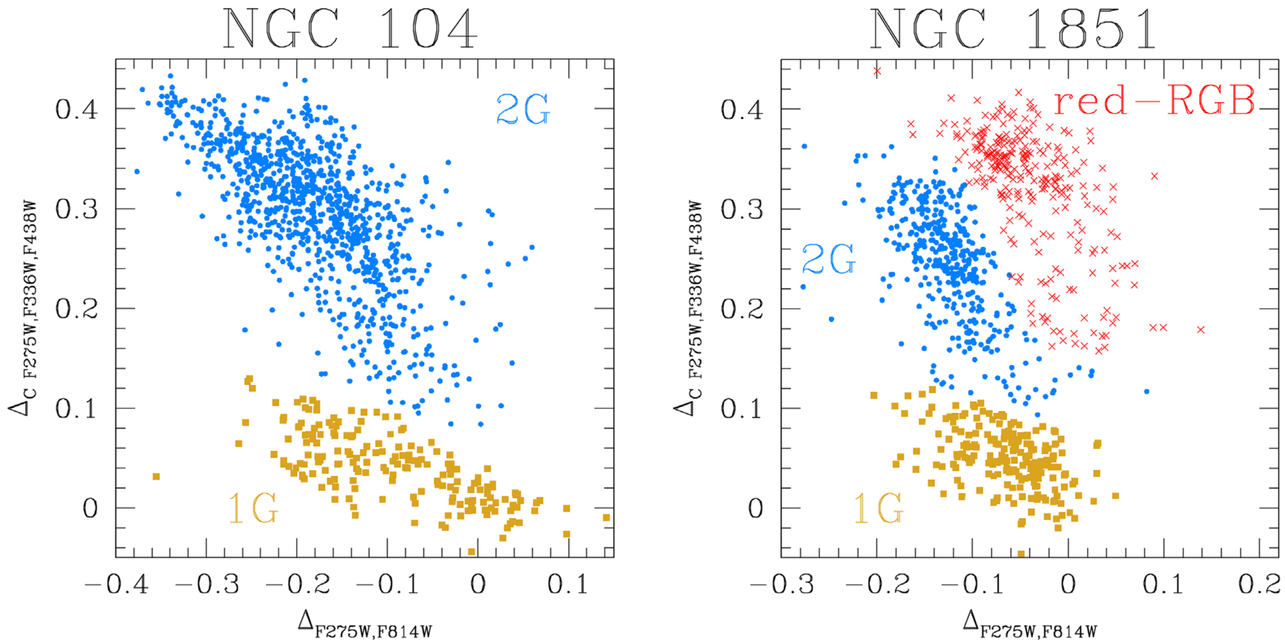

Figure 1. Examples of "chromosome" maps and mPOP tagging for a type-I (NGC 104; left panel) and a type-II (NGC 1851; right panel) GC. In each plot, gold squares and blue dots represent 1G and 2G stars on the red giant branch (RGB), respectively. Red crosses in the right panel highlight the red–RGB stars in NGC 1851.

2. Data Sets, Multiple-population Tagging, and Kinematics

We made use of the PM catalogs[15] of L22, to which we refer for a detailed description of how the PMs were computed.[16] In brief, we designed a multistep reduction to exploit crowded regions, like the cores of GCs, and measured position and flux of sources in HST exposures via effective point-spread function fitting. The geometric-distortion-corrected positions of each object as a function of time were then fit with a least-squares straight line, the slope of which is an estimate of the PM of the star. We cross identified stars in our astrophotometric catalogs with those in the (pseudo) two-color diagrams known as "chromosome maps" of Milone et al. (2017) made for all clusters analyzed in the Treasury GO-13297 program (Piotto et al. 2015). We then applied the astrophotometric quality selections described in both papers to obtain samples of well-measured RGB stars for the mPOP tagging and their kinematic analysis.

The reason for our choice to focus on the RGB stars is twofold. First, the mPOPs along the RGB can be identified more easily because the UV data (which provide the key filters needed for disentangling the mPOPs depending on their CNO contents) used by Milone et al. (2017) were designed to have the highest signal-to-noise ratio (and hence photometric quality) for the RGB stars (see discussion in Piotto et al. 2015). Second, this choice allows us to compare the kinematics of stars with similar masses.

However, focusing on RGB stars necessarily implies small number statistics, and this poses a problem if we choose to work with each cluster separately, computing the velocity dispersions for stars in each mPOP first, and then collecting all measurements from all GCs to study the average kinematic trends of mPOPs. For clusters with different population sizes, the velocity dispersion representing the kinematics of stars at a given distance from the center of the cluster could be obtained by considering stars over a different radial interval. This could potentially introduce a bias that can wash out some of the features we are looking for. For this reason, we instead normalized positions and PMs of the RGB stars in each GC catalog by the GC's half-light radius[17] ($r_{\rm h}$) and central velocity dispersion σ_μ (from L22), respectively. The errors on the central σ_μ were included in the normalized-PM error budget. This normalization allowed us to jointly compare pairs of stellar positions and PMs from all clusters at once, thus increasing the number of data points that can be used to study the kinematics of each mPOP without the drawback discussed before.

Milone et al. (2017) classifies GCs in two main families. Most GCs belong to the type-I family, and are characterized by chromosome maps with two distinct groups[18] made by 1G and 2G stars (left panel of Figure 1).

The remaining clusters are instead labeled as type-II GCs. These systems are present: more complex chromosome maps, where the 1G and 2G stars seem to be divided into subgroups (right panel of Figure 1) and split subgiant branches and RGBs (hereafter red–RGBs) clearly visible in color-magnitude diagrams (CMDs) with specific color combinations.

Stars belonging to the red–RGB population are typically enriched in the overall CNO content, iron and s-element abundances, and have their own 1G and 2G subdivision (hereafter, 1Gr and 2Gr, respectively). We refer to Marino et al. (2019) for

[15] Catalogs are available at MAST as a high level science product via doi:10.17909/jpfd-2m08. See also: https://archive.stsci.edu/hlsp/hacks.

[16] Since our focus is on GCs, we excluded the open cluster NGC 6791 from the investigation.

[17] Cluster parameters (half-light radius, distance, half-mass relaxation time, average perigalactic distance) are taken from the GC database at https://people.smp.uq.edu.au/HolgerBaumgardt/globular/ of Holger Baumgardt (Sollima & Baumgardt 2017; Baumgardt et al. 2020; Baumgardt & Vasiliev 2021; Vasiliev & Baumgardt 2021). Ages are from Dotter et al. (2010), Milone et al. (2014), and Koch & McWilliam (2014). See L22 for details.

[18] Note that 1G stars in type-I GCs present a color spread in the chromosome maps likely due to a spread in Fe of $\gtrsim$0.1 dex (Marino et al. 2019; Lardo et al. 2022; Legnardi et al. 2022).

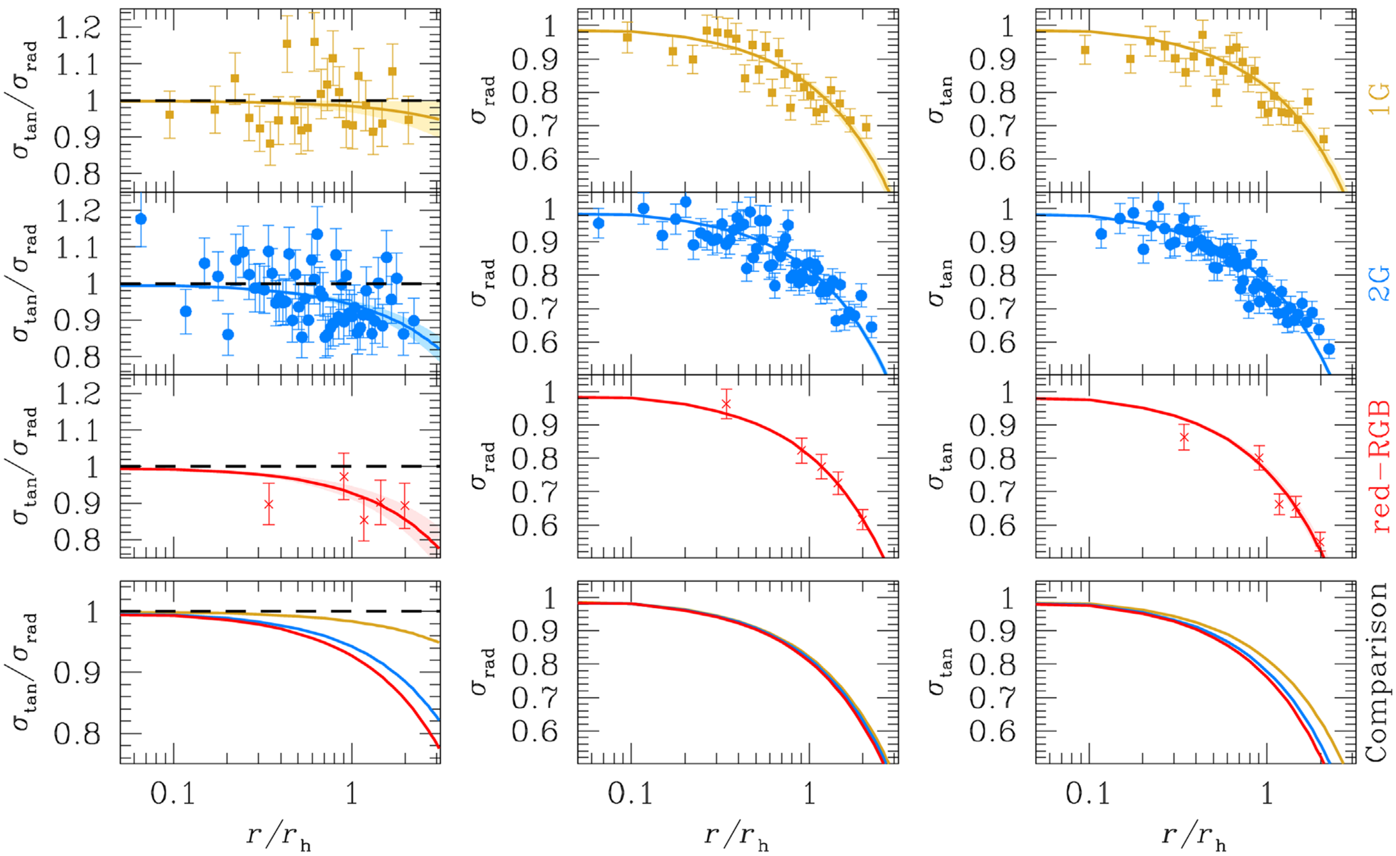

Figure 2. Anisotropy (left), normalized σ_{rad} (center), and σ_{tan} (right) as a function of distance from the center of the cluster in units of r_h. Gold squares (top panel), blue dots (second panel from the top), and red crosses (third panel from the top) represent the 1G, 2G, and red–RGB populations, respectively. The black, dashed horizontal lines in the left panels mark the isotropic case. The solid lines in each panel, color coded as the corresponding points, are least-squares straight-line fits (in linear units of r/r_h) to the points forced to have the ordinate equal to 1 at the center ($r/r_h = 0$). The light-color shaded regions correspond to the 1σ errors of the fits. The comparisons between the trends in each case are shown in the bottom panels (1σ errors of the fits are not plotted for clarity).

a comprehensive description of the spectrophotometric properties of these stars. The origin of these red–RGB stars is not clear. For example, Marino et al. (2019) suggested two possible options: (i) after the gas from which the "classical" 1G and 2G stars formed was almost exhausted, the clusters reaccreted pristine gas that was enriched in iron by supernovae; or (ii) the type-II GCs formed within a dwarf galaxy, with 1G/2G and 1Gr/2Gr born at different times and/or places.

The 1Gr/2Gr distinction is not always as clear as that between the 1G/2G stars in our chromosome maps, in particular for NGC 1851 and NGC 6715. Nevertheless, we arbitrarily divided the red–RGB group is our type-II clusters in 1Gr and 2Gr stars similarly to what was done for 1G and 2G stars in Figure 1. The majority of the red–RGB stars belong to the 2Gr group, and only 219 stars are part of the 1Gr group. Because the photometric tagging of 1Gr and 2Gr stars is not straightforward in our sample of type-II GCs, and given the very few 1Gr stars, we choose to analyze the red–RGB stars as a whole.[19]

Following this classification, we divided our samples in either two (1G and 2G for type-I GCs) or three (1G, 2G, and red–RGB for type-II GCs) subpopulations. The mPOP tagging was directly performed on the chromosome map.

[19] The kinematic analysis shown in Figure 2 provides consistent results for 1Gr, 2Gr and 1Gr+2Gr stars.

3. Global Kinematic Properties of Multiple Populations

As shown in a number of theoretical studies, the velocity anisotropy may provide various fundamental insights into the formation and evolution of GCs (e.g., Tiongco et al. 2016a; Breen et al. 2017, 2021; Pavlík & Vesperini 2021, 2022) and their mPOPs (Tiongco et al. 2019; Vesperini et al. 2021).

We computed the normalized radial and tangential velocity dispersions (σ_{rad} and σ_{tan}, respectively) in equally populated radial bins of at least 200 stars each[20] as in Section 4 of L22, using a maximum-likelihood approach. The left panels of Figure 2 present the anisotropy as a function of radial distance from the center of the cluster in units of r_h for 1G, 2G, and red–RGB stars. The solid lines in each panel, color coded as the corresponding points, are least-squares straight-line fits to the points forced to have the ordinate equal to 1 at the center ($r/r_h = 0$), i.e., $(\sigma_{tan}/\sigma_{rad})(r) = 1 + m \times r/r_h$. These fits are linear in r/r_h, thus they appear curved in our plots with a logarithmic scale on the x-axis. The 1G stars (gold points) in our fields are isotropic even outside 1 r_h, with only a marginal ($\sim 1\sigma$) signature of a radial anisotropy in the outermost part of the field. The 2G (blue) and red–RGB (red) populations are isotropic in the center and become progressively radially anisotropic further from the GC's center. Table 1 collects the median values of the anisotropy for each population for

[20] For the analysis of the kinematics of red–RGB stars in GCs with different dynamical ages, we made at least one radial bin with all stars at disposal when not enough stars were available.

Table 1
Median Anisotropy of 1G, 2G, and red–RGB Stars for Stars with $r > 0.6\ r_h$ and Statistical Significance of the Difference between the mPOP Anisotropies for the Various Cases Discussed in Text

	1G (*N*)	2G (*N*)	red–RGB (*N*)	1G versus 2G	1G versus red–RGB	2G versus red–RGB
		Median Anisotropy			Comparison	
Entire sample	1.02 ± 0.02 (5962)	0.91 ± 0.01 (13884)	0.90 ± 0.03 (1317)	4.9σ	3.3σ	0.3σ
$\mathrm{Age}/t_h \geqslant 10$	1.02 ± 0.03 (1138)	0.95 ± 0.02 (2289)	...	1.9σ	...	...
$7 \leqslant \mathrm{age}/t_h < 10$	1.02 ± 0.06 (885)	0.97 ± 0.02 (1745)	...	0.8σ	...	...
$\mathrm{Age}/t_h < 7$	0.98 ± 0.03 (3939)	0.92 ± 0.02 (9850)	0.90 ± 0.07 (940)	1.6σ	1.0σ	0.3σ
$R_{peri} \leqslant 3.5$ kpc	1.01 ± 0.03 (2479)	0.94 ± 0.02 (6929)	...	1.9σ	...	...
$R_{peri} > 3.5$ kpc	0.94 ± 0.07 (1460)	0.91 ± 0.03 (2921)	...	0.4σ	...	...

Note. The values between brackets in the second, third, and fourth columns are the number of stars used in each case. No number is provided when no stars are available, or if the anisotropy for the specific case was not computed (see text for details).

Table 2
Slopes *m* of the Least-squares Straight-line Fits (in Linear Units of r/r_h) to the Anisotropy Profiles of 1G, 2G, and red–RGB Stars, and Statistical Significance of the Difference between the mPOP Slopes for the Various Cases Discussed in Text

	1G	2G	red–RGB	1G versus 2G	1G versus red–RGB	2G versus red–RGB
		Slope			Comparison	
Entire sample	−0.02 ± 0.02	−0.06 ± 0.01	−0.07 ± 0.02	1.8σ	1.8σ	0.4σ
$\mathrm{Age}/t_h \geqslant 10$	0.02 ± 0.03	−0.05 ± 0.01	...	2.2σ	...	...
$7 \leqslant \mathrm{age}/t_h < 10$	−0.01 ± 0.04	−0.03 ± 0.02	...	0.4σ	...	...
$\mathrm{Age}/t_h < 7$	−0.02 ± 0.02	−0.06 ± 0.01	−0.10 ± 0.03	1.8σ	2.2σ	1.3σ
$R_{peri} \leqslant 3.5$ kpc	−0.01 ± 0.02	−0.06 ± 0.02	...	1.8σ	...	...
$R_{peri} > 3.5$ kpc	−0.05 ± 0.03	−0.08 ± 0.02	...	0.7 σ	...	...

$r > 0.6\ r_h$. This threshold was chosen as a compromise between having enough points to compute a robust median anisotropy value for each mPOP and being sufficiently far from the center of the cluster to capture indications of anisotropy. Table 2 collects the slopes of the straight-line fits. There is a clear difference in the median anisotropy between 1G and 2G stars at the ∼5σ level, and between 1G and red–RGB stars at the ∼3σ level. The slopes of the straight-line fits provide similar results, although the statistical significance is smaller (∼2σ).

These findings are in general agreement with the predictions of numerical models of the evolution of multiple-population clusters (see, e.g., Vesperini et al. 2021). Specifically, theoretical models explain these behaviors as the consequence of the initial spatial differences between 1G and 2G stars. Simulations usually start with a 2G population more centrally concentrated in the inner regions of a more diffuse 1G system as suggested by models of formation of mPOPs (D'Ercole et al. 2008; Calura et al. 2019). For systems starting with an isotropic velocity distribution, the anisotropy of the 2G stars is a consequence of the outward diffusion of 2G stars (Tiongco et al. 2016b; Vesperini et al. 2021). For systems starting with an anisotropic velocity distribution, this difference is the result of a more rapid evolution toward a isotropic velocity distribution of 1G stars. In such case, it is also possible to find both populations to be characterized by anisotropic velocity distributions. We point out that although the difference between the anisotropy of 1G and 2G stars is small, its extent is generally consistent with that found in numerical models at the distances from the clusters' centers probed by our data.

The middle and right panels show the radial profiles of the normalized σ_{rad} and σ_{tan}, respectively. All the populations have similar radial velocity dispersions, while tangential velocity dispersions are larger for 1G stars than for 2G and red–RGB sources. These findings are in agreement with the theoretical predictions for which the different degrees of radial anisotropy between 1G and 2G stars is caused by a difference in the tangential component of their motions, rather than in the radial component (Bellini et al. 2015; Vesperini et al. 2021).

In Figure 3, we further explore the anisotropy of mPOPs for GCs with different dynamical ages as measured by the ratio of the GCs' ages to their half-mass relaxation time (t_h). L22 found that dynamically old ($\mathrm{age}/t_h > 10$) and young ($\mathrm{age}/t_h < 7$) GCs are characterized by different velocity distributions at r_h. We followed this same classification to better highlight differences and analogies between 1G and 2G stars. Figure 3 presents the anisotropy as a function of distance from the center of the cluster in units of r_h for dynamically old (top), intermediate (second from the top), and young (third from the top) GCs. The bottom panels show the comparison between the trends of each mPOP in GCs with different dynamical ages, while the rightmost panels collect the straight-line fits for each population for GCs with the same the dynamical age. The trends shown in these panels are consistent with the global trends shown in Figure 2, but the differences between the mPOP anisotropies are less evident (see Tables 1 and 2). Most of the 1G fits are consistent with an isotropic distribution, while most of the 2G median anisotropies and slopes indicate a statistically significant anisotropy. Our analysis suggests that, for a given mPOP, there might be kinematic differences depending on the dynamical age of the hosting cluster, but the large error bars do not allow us to draw any definitive conclusion. Larger differences might be present further from the center of the

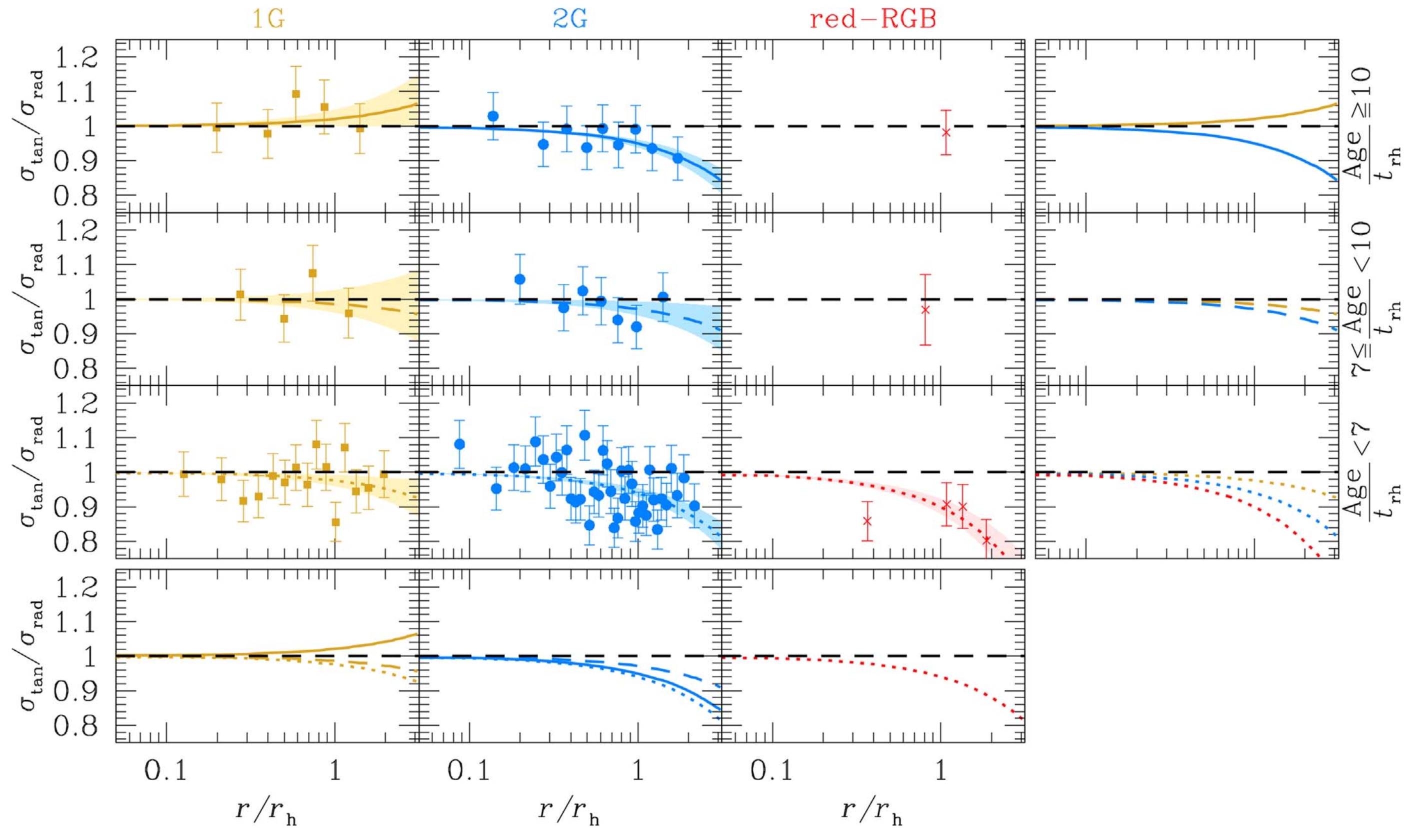

Figure 3. As in the left panels of Figure 2, but dividing the sample of GCs according to their dynamical age (age/$t_{\rm h}$ ratio). The first three columns show the anisotropy for 1G (gold squares), 2G (blue dots), and red–RGB (red crosses), respectively. The black, horizontal lines mark the isotropic case. The lines, colored as the point in the same plot, are a straight-line fit to the data (see details in Figure 2; no line was fit for the red–RGB samples with only one data point). The first three rows present the result for old, intermediate, and young GCs, from top to bottom, respectively. The rightmost panels collect the straight-line fits for each population for GCs with the same the dynamical age, while the panels at the bottom show the comparison between the trends of each mPOP in clusters with different dynamical ages.

cluster, where the relaxation time is longer and fingerprints of the initial kinematic properties might still be detectable. Finally, no conclusion can be inferred for the red–RGB stars in intermediate and old GCs because of the low statistics.

4. Dependence on the Galactic Tidal Field

Previous studies (e.g., Vesperini et al. 2014; Tiongco et al. 2016b; Bianchini et al. 2018) have shown that the external tidal field of the host galaxy may play an important role in the early- and long-term evolution of the velocity anisotropy. In particular, the loss of stars in stronger tidal fields preferentially affects stars on more radial orbits, causing a decrease of the radial anisotropy in the outer regions, and a gradual evolution toward a more isotropic (or even tangential) velocity distribution. We explore the possible role of the external tidal field as a function of perigalactic distances ($R_{\rm peri}$) to quantify how much the Galactic tidal field affects the evolution of GCs.

We have divided clusters into two groups with $R_{\rm peri} > 3.5$ kpc and $R_{\rm peri} \leqslant 3.5$ kpc, respectively. The same value of the pericentric distance was adopted by Zennaro et al. (2019) and Milone et al. (2020) who explored the possible role of the Galactic tidal field on the fraction of 1G stars. Those studies found that the main correlation is between the fraction of 1G stars and the mass of the cluster and that, for a given value of the mass, clusters with larger pericentric distances tend to have larger 1G fractions.

Two-body encounters progressively erase fingerprints of initial kinematic differences between mPOPs. Thus, we focused only on dynamically young GCs (age/$t_{\rm h} < 7$). This choice is also dictated by the properties of the GCs in our sample, given we have no dynamically old and intermediate GCs with $R_{\rm peri} > 3.5$ kpc. Red–RGB stars were excluded because there is only one type-II GC (NGC 6715) with age/$t_{\rm h} < 7$ and large perigalactic distance.

We show the anisotropy profiles for 1G and 2G stars for different $R_{\rm peri}$ in Figure 4. Our analysis suggests that the degree of kinematic anisotropy in 1G and 2G stars does depend on the perigalactic distance. The 1G stars are isotropic at all distances in our fields for $R_{\rm peri} \leqslant 3.5$ kpc, suggesting that the tidal field may have erased any initial anisotropy; the 2G population for clusters with the same pericentric distances, on the other hand, still displays some velocity anisotropy, in general agreement with what is expected in models in which the 2G was initially more centrally concentrated than the 1G and thus less affected by the tidal field (Vesperini et al. 2021). In these clusters, we find that the average anisotropy for 1G and 2G groups at $r > 0.6\, r_{\rm h}$ are 1.01 ± 0.03 and 0.94 ± 0.02, respectively ($\sim 2\sigma$ difference). In the group of clusters with $R_{\rm peri} > 3.5$ kpc, both populations are still characterized by a radially anisotropic velocity distribution, with an average anisotropy at $r > 0.6\, r_{\rm h}$ for 1G and 2G groups of 0.94 ± 0.07 and 0.91 ± 0.03, respectively. While the anisotropy of 2G stars is statistically significant at the 3σ level, that of 1G sources is not as strong because the large error bars make the kinematics of this group consistent with the isotropic case at the $\sim 1\sigma$ level. Similar results can be inferred by comparing the slopes of the corresponding least-squares straight-line fits. Our data show a

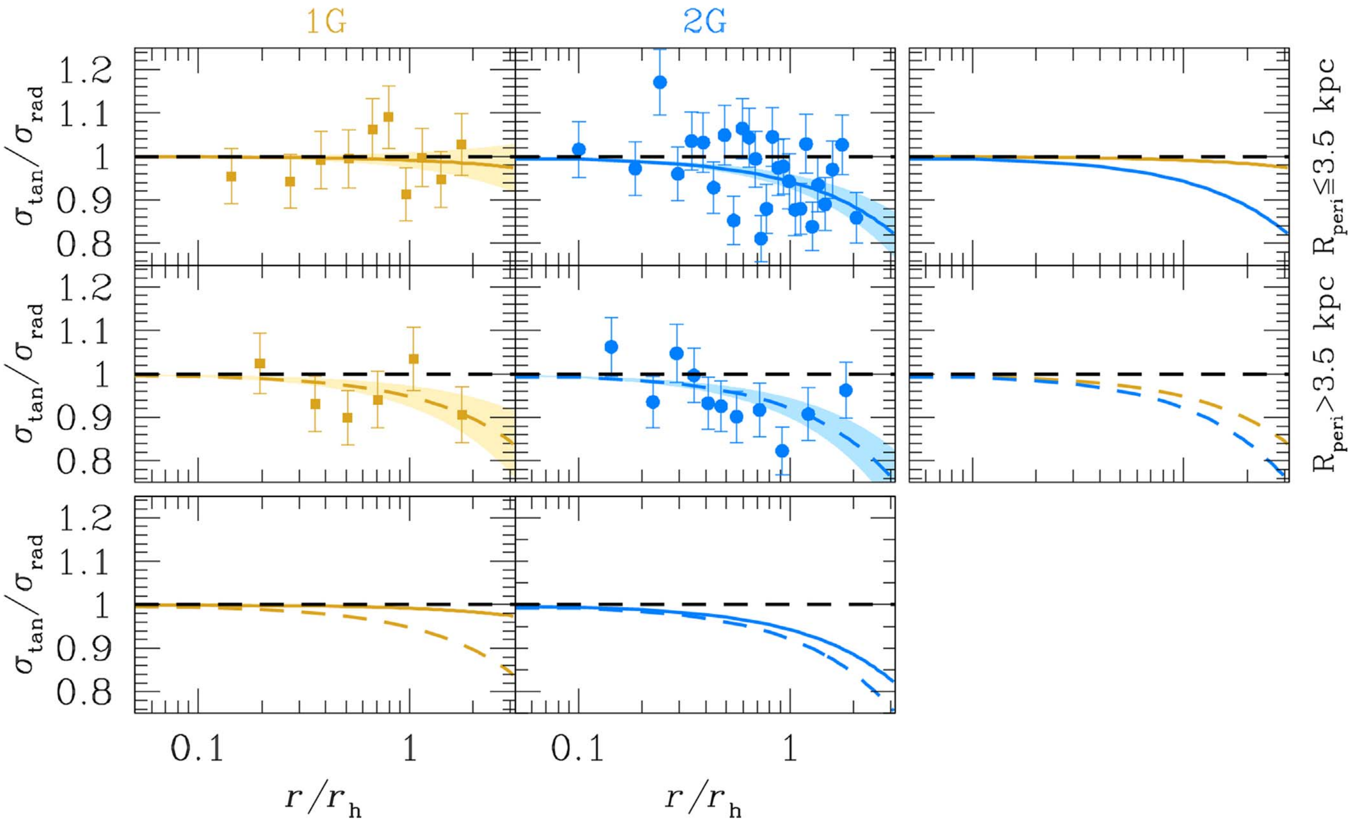

Figure 4. Similarly to Figure 3, we show the anisotropy as a function of distance from the centers of the clusters in units of r_h for mPOPs in clusters with different R_{peri}. The top and middle rows present the 1G (gold) and 2G (blue) anisotropy profiles for GCs with $R_{peri} \leqslant 3.5$ kpc and $R_{peri} > 3.5$ kpc, respectively. The black, horizontal line is set to 1 (isotropic case). The colored lines are a straight-line fit to the data (see details in Figure 2). The comparison between the straight-line fit for mPOPs in GCs with the same R_{peri} is given in the rightmost panels, while between the same mPOP in GCs with different R_{peri} is highlighted in the bottom panels.

marginal difference ($<1\sigma$) between 1G and 2G stars at large r/r_h for clusters in this group, but the possible larger anisotropy of the 2G population in the outer regions of clusters with large R_{peri} needs to be investigated further over broader radial ranges.

Finally, Table 1 shows that the fraction of 1G stars in dynamically young GCs with $R_{peri} < 3.5$ kpc is 0.26, while that in GCs with $R_{peri} > 3.5$ kpc is 0.33. This is qualitatively in agreement with the findings of Zennaro et al. (2019) and Milone et al. (2020), i.e., GCs with larger R_{peri} values tend to have larger 1G fractions.

5. Conclusions

This paper presents the first homogeneous kinematic investigation of mPOPs in 56 GCs. We have focused on bright RGB stars, for which the mPOP tagging is clearer in chromosome maps, and measure the velocity dispersion of 1G and 2G stars. While 1G stars are, in general, kinematically isotropic at both inner and outer radii in our fields, 2G stars are isotropic at the center and progressively become more radially anisotropic further from the center of the cluster. This anisotropy is a reflection of the fact that the 2G stars have the same radial dispersions as the 1G stars, but much lower tangential dispersions. Our study confirms previous results obtained for specific GCs with Gaia (Milone et al. 2018; Cordoni et al. 2020a, 2020b) and HST (Anderson & van der Marel 2010; Richer et al. 2013; Bellini et al. 2015, 2018; Libralato et al. 2018, 2019, 2022; Dalessandro et al. 2021). Our findings are also in general agreement with the theoretical predictions of models that follow the dynamical evolution of mPOPs and show that these properties are expected in systems in which 2G stars formed more centrally concentrated than 1G stars.

Using our sample, we also find possible indications that the Galactic tidal fields affect the kinematic properties of 1G and 2G stars. Specifically, we show that the anisotropy of 1G and 2G stars depends on the perigalactic distance R_{peri} of the host cluster. Systems with large R_{peri} experience, on average, a weaker tidal field and their stars are able to preserve a (stronger) radial anisotropy than GCs with pericentric distances in the innermost regions of the Galaxy (see also Zennaro et al. 2019; Milone et al. 2020, for the possible effect of R_{peri} on the fraction of 1G stars).

Although these results are not conclusive, due to the limited sample and limited radial coverage, our analysis is a step forward toward a complete understanding of the mPOP phenomenon. This initial study provides further motivation for new and deeper surveys with HST, JWST and, in the future, the Nancy Grace Roman Space Telescope, which will be essential to extend the investigation in the almost uncharted outskirts of GCs (Bellini et al. 2019; WFIRST Astrometry Working Group et al. 2019).

The authors thank the anonymous referee for the detailed suggestions that improved the quality of our work. M.L. and A. B. acknowledge support from GO-13297, GO-15857,and GO-16298. E.V. acknowledges support from NSF grant AST-2009193. A.P.M. acknowledges funding from the European Research Council (ERC) under the European Union's Horizon 2020 research innovation program (grant agreement ERC-StG

2016, No 716082 "GALFOR," PI: Milone, http://progetti.dfa.unipd.it/GALFOR). A.A. acknowledges support from the Ministerio de Ciencia e Innovación of Spain (grant PID2020-115981GB-I00), from the Instituto de Astrofísica de Canarias (grant P/309403) and from Khalifa University of Abu Dhabi through project CIRA-2021-65 8474000413. B.B. acknowledges partial financial support from FAPESP, CNPq, and CAPES—financial code 001. A.S. is grateful to the Bjorn Lamborn Endowment for support while some of this work was being done. M.L. thanks LS, GL and LL for their support to complete this project.

This research was pursued in collaboration with the HSTPROMO (High-resolution Space Telescope Proper Motion) collaboration, a set of projects aimed at improving our dynamical understanding of stars, clusters, and galaxies in the nearby universe through measurement and interpretation of proper motions from HST, Gaia, and other space observatories. We thank the collaboration members for the sharing of their ideas and software.

Based on observations with the NASA/ESA HST, obtained at the Space Telescope Science Institute, which is operated by AURA, Inc., under NASA contract NAS 5-26555. This research made use of `astropy`, a community-developed core `python` package for Astronomy (Astropy Collaboration et al. 2013, 2018, 2022), and `emcee` (Foreman-Mackey et al. 2013).

ORCID iDs

Mattia Libralato https://orcid.org/0000-0001-9673-7397
Enrico Vesperini https://orcid.org/0000-0003-2742-6872
Andrea Bellini https://orcid.org/0000-0003-3858-637X
Antonino P. Milone https://orcid.org/0000-0001-7506-930X
Roeland P. van der Marel https://orcid.org/0000-0001-7827-7825
Giampaolo Piotto https://orcid.org/0000-0002-9937-6387
Jay Anderson https://orcid.org/0000-0003-2861-3995
Antonio Aparicio https://orcid.org/0000-0002-6054-0004
Beatriz Barbuy https://orcid.org/0000-0001-9264-4417
Luigi R. Bedin https://orcid.org/0000-0003-4080-6466
Thomas M. Brown https://orcid.org/0000-0002-1793-9968
Santi Cassisi https://orcid.org/0000-0001-5870-3735
Domenico Nardiello https://orcid.org/0000-0003-1149-3659
Ata Sarajedini https://orcid.org/0000-0001-6708-4374
Michele Scalco https://orcid.org/0000-0001-8834-3734

References

Anderson, J., & van der Marel, R. P. 2010, ApJ, 710, 1032
Astropy Collaboration, Price-Whelan, A. M., Sipőcz, B. M., et al. 2018, AJ, 156, 123
Astropy Collaboration, Price-Whelan, A. M., Lim, P. L., et al. 2022, ApJ, 935, 167
Astropy Collaboration, Robitaille, T. P., Tollerud, E. J., et al. 2013, A&A, 558, A33
Bastian, N., & Lardo, C. 2018, ARA&A, 56, 83
Baumgardt, H., Sollima, A., & Hilker, M. 2020, PASA, 37, e046
Baumgardt, H., & Vasiliev, E. 2021, MNRAS, 505, 5957
Bellini, A., Libralato, M., Anderson, J., et al. 2019, Astro2020: Decadal Survey on Astronomy and Astrophysics, Science White Paper No., 173
Bellini, A., Libralato, M., Bedin, L. R., et al. 2018, ApJ, 853, 86
Bellini, A., Vesperini, E., Piotto, G., et al. 2015, ApJL, 810, L13
Bianchini, P., Webb, J. J., Sills, A., & Vesperini, E. 2018, MNRAS, 475, L96
Breen, P. G., Rozier, S., Heggie, D. C., & Varri, A. L. 2021, MNRAS, 502, 4762
Breen, P. G., Varri, A. L., & Heggie, D. C. 2017, MNRAS, 471, 2778
Calura, F., D'Ercole, A., Vesperini, E., Vanzella, E., & Sollima, A. 2019, MNRAS, 489, 3269
Cassisi, S., & Salaris, M. 2020, A&ARv, 28, 5
Cordoni, G., Milone, A. P., Mastrobuono-Battisti, A., et al. 2020a, ApJ, 889, 18
Cordoni, G., Milone, A. P., Marino, A. F., et al. 2020b, ApJ, 898, 147
Dalessandro, E., Lapenna, E., Mucciarelli, A., et al. 2016, ApJ, 829, 77
Dalessandro, E., Raso, S., Kamann, S., et al. 2021, MNRAS, 506, 813
D'Ercole, A., Vesperini, E., D'Antona, F., McMillan, S. L. W., & Recchi, S. 2008, MNRAS, 391, 825
Dotter, A., Sarajedini, A., Anderson, J., et al. 2010, ApJ, 708, 698
Foreman-Mackey, D., Hogg, D. W., Lang, D., & Goodman, J. 2013, PASP, 125, 306
Gratton, R., Bragaglia, A., Carretta, E., et al. 2019, A&ARv, 27, 8
Gratton, R. G., Carretta, E., & Bragaglia, A. 2012, A&ARv, 20, 50
Koch, A., & McWilliam, A. 2014, A&A, 565, A23
Lagioia, E. P., Milone, A. P., Marino, A. F., & Dotter, A. 2019, ApJ, 871, 140
Lardo, C., Salaris, M., Cassisi, S., & Bastian, N. 2022, A&A, 662, A117
Larsen, S. S., Brodie, J. P., Grundahl, F., & Strader, J. 2014, ApJ, 797, 15
Legnardi, M. V., Milone, A. P., Armillotta, L., et al. 2022, MNRAS, 513, 735
Libralato, M., Bellini, A., Piotto, G., et al. 2019, ApJ, 873, 109
Libralato, M., Bellini, A., van der Marel, R. P., et al. 2018, ApJ, 861, 99
Libralato, M., Bellini, A., Vesperini, E., et al. 2022, ApJ, 934, 150
Marino, A. F., Milone, A. P., Renzini, A., et al. 2019, MNRAS, 487, 3815
Martocchia, S., Dalessandro, E., Lardo, C., et al. 2019, MNRAS, 487, 5324
Milone, A. P., & Marino, A. F. 2022, Univ, 8, 359
Milone, A. P., Marino, A. F., Da Costa, G. S., et al. 2020, MNRAS, 491, 515
Milone, A. P., Marino, A. F., Dotter, A., et al. 2014, ApJ, 785, 21
Milone, A. P., Marino, A. F., Mastrobuono-Battisti, A., & Lagioia, E. P. 2018, MNRAS, 479, 5005
Milone, A. P., Piotto, G., Renzini, A., et al. 2017, MNRAS, 464, 3636
Nardiello, D., Piotto, G., Milone, A. P., et al. 2019, MNRAS, 485, 3076
Niederhofer, F., Bastian, N., Kozhurina-Platais, V., et al. 2017, MNRAS, 465, 4159
Pavlík, V., & Vesperini, E. 2021, MNRAS, 504, L12
Pavlík, V., & Vesperini, E. 2022, MNRAS, 509, 3815
Piotto, G., Milone, A. P., Bedin, L. R., et al. 2015, AJ, 149, 91
Renzini, A., D'Antona, F., Cassisi, S., et al. 2015, MNRAS, 454, 4197
Richer, H. B., Heyl, J., Anderson, J., et al. 2013, ApJL, 771, L15
Sollima, A., & Baumgardt, H. 2017, MNRAS, 471, 3668
Tiongco, M. A., Vesperini, E., & Varri, A. L. 2016a, MNRAS, 461, 402
Tiongco, M. A., Vesperini, E., & Varri, A. L. 2016b, MNRAS, 455, 3693
Tiongco, M. A., Vesperini, E., & Varri, A. L. 2019, MNRAS, 487, 5535
Vasiliev, E., & Baumgardt, H. 2021, MNRAS, 505, 5978
Vesperini, E., Hong, J., Giersz, M., & Hypki, A. 2021, MNRAS, 502, 4290
Vesperini, E., Varri, A. L., McMillan, S. L. W., & Zepf, S. E. 2014, MNRAS, 443, L79
WFIRST Astrometry Working Group, Sanderson, R. E., Bellini, A., et al. 2019, JATIS, 5, 044005
Zennaro, M., Milone, A. P., Marino, A. F., et al. 2019, MNRAS, 487 3239